PNAS RESEARCH ARTICLE | EARTH, ATMOSPHERIC, AND PLANETARY SCIENCES OPEN ACCESS

Heterogeneous iodine-organic chemistry fast-tracks marine new particle formation

Ru-Jin Huang[a,b,c,d,1], Thorsten Hoffmann[e], Jurgita Ovadnevaite[f], Ari Laaksonen[g,h], Harri Kokkola[g], Wen Xu[i,j], Wei Xu[a,f], Darius Ceburnis[f], Renyi Zhang[i,j], John H. Seinfeld[k,l], and Colin O'Dowd[f]

Edited by Akkihebbal Ravishankara, Colorado State University, Fort Collins, CO; received January 30, 2022; accepted June 14, 2022

The gas-phase formation of new particles less than 1 nm in size and their subsequent growth significantly alters the availability of cloud condensation nuclei (CCN, >30–50 nm), leading to impacts on cloud reflectance and the global radiative budget. However, this growth cannot be accounted for by condensation of typical species driving the initial nucleation. Here, we present evidence that nucleated iodine oxide clusters provide unique sites for the accelerated growth of organic vapors to overcome the coagulation sink. Heterogeneous reactions form low-volatility organic acids and alkylaminium salts in the particle phase, while further oligomerization of small α-dicarbonyls (e.g., glyoxal) drives the particle growth. This identified heterogeneous mechanism explains the occurrence of particle production events at organic vapor concentrations almost an order of magnitude lower than those required for growth via condensation alone. A notable fraction of iodine associated with these growing particles is recycled back into the gas phase, suggesting an effective transport mechanism for iodine to remote regions, acting as a "catalyst" for nucleation and subsequent new particle production in marine air.

marine new particle formation | heterogeneous reaction | iodine | intermediate oxidized organics

Marine aerosol formation contributes significantly to the global radiative budget given the high susceptibility of marine stratiform cloud radiative properties to changes in cloud condensation nuclei (CCN) availability. Atmospheric new-particle-formation is thought to involve nucleation of sulfuric acid with water, ammonia, or amines followed by condensation/growth in the presence of organic vapors (1, 2). Unique in the marine boundary layer (MBL), new particle formation involves sequential addition of HIO_3 or clustering of iodine oxides (I_xO_y) (3, 4). In specific source regions such as coastal zones, seaweed beds, or snowpack/pack-ice, iodine oxide nucleation can be a driving force for nucleation (5–7). Over Arctic waters, nonetheless, one study finds insufficient iodic acid vapors to grow nucleated particles to CCN sizes (8), whereas another study finds that both nucleation and growth are almost exclusively driven by iodic acid (9). Over the open ocean, the supply of iodine oxides has been thought to be limited; however, recent measurements suggest that significant reactive iodine chemistry can occur in these regions (10). Moreover, observational evidence exists for open ocean particle formation and growth, especially when oceanic productivity is high (11, 12). An increase in atmospheric iodine levels in the North Atlantic since the mid-20th century has been shown to be driven by growth of anthropogenic ozone and enhanced subice phytoplankton production (13). While the reported IO concentration (0.4–3.1 ppt) in the remote MBL (10, 14, 15) is likely sufficient for formation of prenucleation clusters (~1 nm), growth of these initial clusters requires the presence of other condensable vapors (16). Since preexisting aerosol particles act as a strong sink for the nucleated clusters, thus inhibiting atmospheric aerosol and CCN formation (17, 18), this early growth phase is essential for their survival. Whereas sulfuric acid vapor is also involved in nucleation, its level in remote open ocean is generally too low (10^5 molecules cm^{-3}) to support subsequent particle growth, leaving organic vapors as the most plausible alternative for particle growth.

In the marine atmosphere, condensing organics must originate from the oxidation of marine volatile organic compounds (VOCs), which predominantly comprise C_1–C_5 VOCs (e.g., isoprene) released from phytoplankton. Principal high volatility oxidation products consist of intermediate oxidized organics (IOOs), such as polyhydric alcohols (e.g., tetrols) or polyfunctional carbonyls (e.g., glyoxal) (19–22). Nonetheless, growth of available prenucleation clusters/nanometer particles requires condensing organic molecules of low effective volatilities (i.e., saturation mass concentration, $C^* < \sim 10^{-3}$ μg m^{-3}); otherwise, preferential condensation of the organic mass to larger-diameter particles would occur (23, 24). Formation of such extremely low-volatility organic compounds (ELVOCs) from gas-phase reaction is well established for monoterpene oxidation products (25, 26).

Significance

Unique in the marine boundary layer, new particle formation involves iodine-oxide nucleation; however, challenges remain in explaining the growth. Condensation of organic vapors has been suggested as the most probable mechanism, but condensation growth requires condensing organic molecules of low effective volatilities. Here, we show, through a combination of laboratory experiments, ambient field measurements, and model studies, that exposure of iodine-oxide nanoparticles to organic vapors may lead to accelerated particle growth through heterogeneous reactions forming low-volatility organic acids and alkylaminium salts in the particle phase. Moreover, we show that a notable fraction of iodine is recycled back into the gas phase during particle growth, providing insights into iodine-organic multiphase reactions for marine new particle formation.

Author contributions: R.-J.H., T.H., and C.O. designed research; R.-J.H., J.O., Wen Xu, and D.C. performed research; R.Z. contributed new reagents/analytic tools; R.-J.H., J.O., A.L., H.K., Wei Xu, and D.C. analyzed data; and R.-J.H., T.H., J.H.S., and C.O. wrote the paper.

The authors declare no competing interest.

This article is a PNAS Direct Submission.

[1]To whom correspondence may be addressed. Email: rujin.huang@ieecas.cn.

This article contains supporting information online at http://www.pnas.org/lookup/suppl/doi:10.1073/pnas.2201729119/-/DCSupplemental.

Published August 2, 2022.

A potential pathway for formation of low-volatility organics could also result from particle-phase chemical reactions induced by iodine oxides in the early stages of marine particle formation. When the underlying chemistry is sufficiently fast, kinetic condensation occurs, resulting in particles with diameters smaller than about 50 nm growing at the same rate (e.g., nm h^{-1}) (24). If, however, particle-phase chemistry is preferentially favored in the smallest particles (i.e., stemming from the higher relative concentration of iodine oxides in freshly formed marine particles), growth of the nucleated particles could proceed more rapidly, as compared to that in which gas-phase chemistry is the source of the low-volatility compounds (23).

In this paper, we present experimental results from field measurements as well as laboratory studies of nanometer particle growth and derive a plausible chemical mechanism from the results that can explain the observations of ultrafine particle growth in the marine atmosphere. The results suggest that both iodine and condensed organics contribute to particle growth from a nascent nucleation mode into an ultrafine particle mode. Moreover, laboratory studies of the growth of seed iodine oxide particles (IOP) via heterogeneous reactions with organic vapors suggest a hitherto unrecognized mechanism that fast-tracks the growth of nucleation mode clusters into survivable aerosol particles. In this process, a notable fraction of the iodine associated with these growing particles is recycled back to the gas phase, suggesting a transport mechanism for iodine to remote regions.

Results

Ultrafine Particle Growth Driven by Heterogeneous Reactions. At the Mace Head Global Atmosphere Watch Research Station, located on the west coast of Ireland, over a period of 10 y (2008–2018), we observed over 80 open ocean new particle formation events with steady growth lasting longer than 6 h under clean marine conditions. These events occurred in marine air masses with 57% of occurrence in maritime Polar (*mP*), 36% of maritime Arctic (*mA*), and 17% of maritime Tropical (*mT*) air masses. *SI Appendix*, Fig. S1 shows the geographical distribution of air mass backward trajectory frequency. For the most frequently occurring *mP* air masses, there are no exceptional conditions associated with these events. The event, discussed in this study, is a typical *mP* event occurring in June 2012 and lasting for over 36 h, characteristics of which were summarized by O'Dowd et al. (11). Almost all of the open ocean new particle formation events occurred in *mP* masses delineate southern boundaries of low-pressure systems guided eastward by the Polar jet across the North Atlantic Ocean. The *mP* air masses as depicted in *SI Appendix*, Fig. S2 typically contain small cumulus structures sometimes spreading into broken stratocumulus as the cold air advects over warmer water. In these air masses, it is not uncommon for the cumuli to release precipitation that reaches the surface, resulting in some inhomogeneity in both the surface and the decoupled subcloud layer—tends to buffer mixing between the surface layer and the free troposphere (*SI Appendix*, Fig. S3)—often evidenced in the low cloud fraction.

The boundary layer in *mP* air masses is typically meteorologically unstable, leading to vertical mixing typically limited to the boundary layer, but is rather well mixed and capped by a residual layer, resulting in pseudostationary periods where particle production and growth can be sustained for many hours. Those air masses have typically low cloud fraction and when passing over biologically rich and low wind waters favor secondary particle production. The chemical composition of a growing nascent ultrafine particle mode in an *mP* air mass advecting over the North East Atlantic is illustrated in Fig. 1. The nascent ultrafine mode is observed with a modal diameter of ~30 nm growing to ~60 nm over a 36-h period (Fig. 1*A*). The physical properties, growth rates, and frequency of occurrence of such events have been previously reported (11); however, to date, the chemical composition of such a growing mode in marine air has not been characterized. Here, using an Aerodyne high resolution time of flight aerosol mass spectrometer (HR-ToF-AMS), we find the ultrafine mode comprises organics, sulfate, methanesulfonic acid (MSA), ammonium, and iodine, with organics contributing predominantly to the growth (see Fig. 1*B* and *SI Appendix*, Fig. S4). Since MSA contribution was <10%, it was not separated from sulfate and organics in further discussion. While the sulfate diameter increases with particle growth, the ultrafine mode amplitude stays relatively the same. In contrast, organics show an increase in both diameter and amplitude. This has resulted in organics contributing 60% to the growth of the ultrafine mode, while sulfate contributed 25% and the remaining mass came from MSA (9%) and ammonium (6%). This bimodal mass distribution is confirmed by the mass distribution (density of 1.5 g cm^{-3}) from scanning mobility particle sizer (SMPS) measurements and shows reasonable agreement for both ultrafine and accumulation modes in mass and diameter (Fig. 1*B*). Moreover, the presence of iodine in the ultrafine aerosol mode is confirmed by high-resolution AMS measurements (*SI Appendix*, Fig. S4).

To investigate the hypothesis that organic vapors contribute to IOP growth, and to explore the role of heterogeneous reactions in such growth as well, we performed a set of laboratory experiments. A nano-tandem differential mobility analyzer (DMA) was employed to determine quantitatively the growth of monodisperse seed IOPs in the size range of 6–20 nm on exposure to organic vapors. Prominent organic vapors in the marine atmosphere were studied, including meso-erythritol (a tetrol that serves as a surrogate for isoprene oxidation products), glyoxal, and dimethylamine. The DMA-system strips out a narrow-band monodisperse seed particle of diameter D_P^* in the first DMA for exposure to organic vapors, followed by measurement of the diameter after exposure, D_P, by the second DMA. The ratio of measured particle sizes (D_P/D_P^*) from the DMAs constitutes the growth-factor. Fig. 2 *A* and *B* illustrate the growth-factors on exposure of IOPs to individual organic vapors, reaching values as high as 1.3 for seed nanoparticles 6–20 nm in size.

The observed particle growth is a result of heterogeneous reactions that form low-volatility particle-phase organic acids and alkylaminium salts. Moreover, oligomerization of small α-dicarbonyls (e.g., glyoxal) also contributes to the growth of ultrafine particles (27). The formation of low-volatility organic acids was confirmed by analyzing the chemical composition of nanoparticles using a thermal desorption-ion drift chemical ionization mass spectrometer (TD-ID-CIMS, see *SI Appendix*, Fig. S5). Meso-tartaric acid was identified in nanoparticles exposed to meso-erythritol with a desorption mass spectrum revealing a protonated tartaric acid with a loss of H_2O (m/z 133, $[C_4H_6O_6 + H - H_2O]^+$, *SI Appendix*, Fig. S5*A*) in positive MS mode and a negatively charged tartaric acid via reaction with reagent ions CO_3^-/CO_4^- (m/z 182, $([C_4H_6O_6 + O_2]^-$, *SI Appendix*, Fig. S5*B*) in negative MS mode, respectively. For exposure to glyoxal, the desorption mass spectrum was characterized by deprotonated glyoxylic acid (m/z 73, $[C_2H_2O_3 - H]^-$, *SI Appendix*, Fig. S5*C*) and deprotonated oxalic acid (m/z 89, $[C_2H_2O_4 - H]^-$, *SI Appendix*, Fig. S5*D*). Moreover, oxalic acid has been observed in the particle phase in

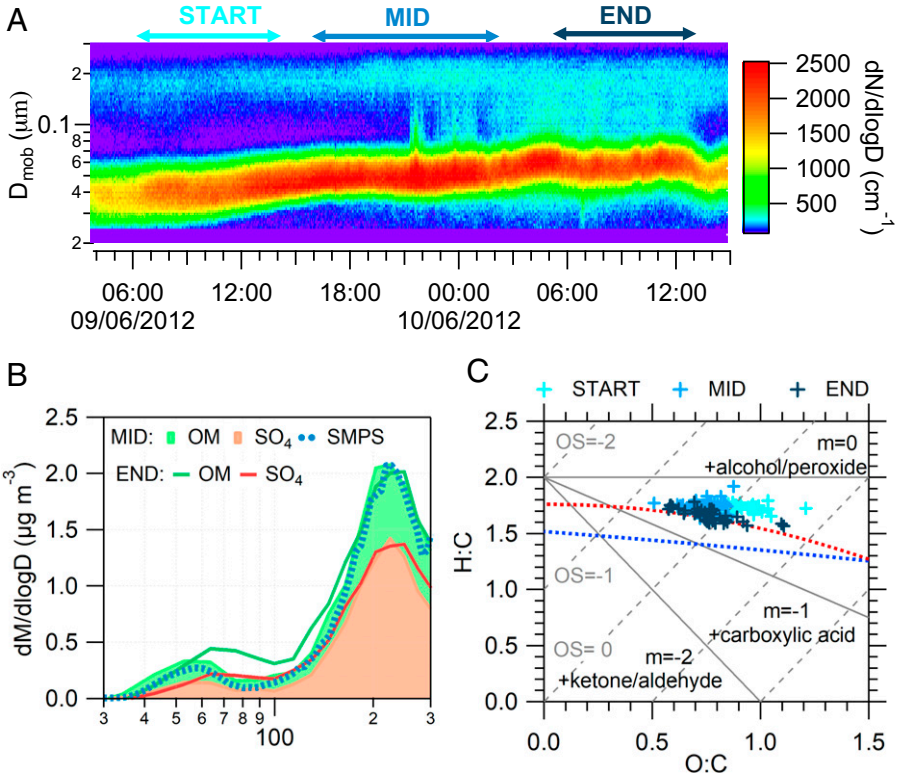

Fig. 1. Example of a typical growing nascent ultrafine particle event observed at the Mace Head Global Atmosphere Watch Research Station, located on the west coast of Ireland in June 2012. This event, manifested in the maritime Polar air mass as derived from 3-d back trajectories and lasted for over 36 h, is a typical open ocean event as reported in a statistical study (11) and regularly observed at Mace Head and over the North Atlantic. (*A*) Time trend of SMPS size distribution with the periods indicating different stages of the event (start, middle, and end). (*B*) Chemical speciation of ultrafine and accumulation mode particles by the AMS for MID and END stages and SMPS mass distribution (with density of 1.5 g cm^{-3}) for the MID stage. Note that in order to be consistent with the SMPS measurements, AMS-derived vacuum aerodynamic diameter has been converted to mobility diameter. (*C*) Van Krevelen diagram for the total organic matter during an ultrafine event. Different colors represent stages of the event. Gray lines represent functionalization reactions of the organic species (41).

Northeast Atlantic MBL (28), exhibiting a seasonal trend similar to that of IOP formation, suggesting the occurrence of oxidation of glyoxal by higher iodine oxides in the marine atmosphere. This IOP oxidation mechanism may provide an explanation for the missing source of oxalic acid, relative to ambient observations (29).

We also observed substantial increases in IOP nanoparticle growth-factors exposed to a mixture of meso-erythritol (or glyoxal) and dimethylamine vapors. The growth-factor, reaching 1.7 for the larger seed particles, exceeds the aggregated growth-factors stemming from exposure to individual organic vapors alone (Fig. 2 *A* and *B*). This behavior can be attributed to a stepwise accretion of the basic molecules (e.g., dimethylamine) concomitant with the addition of organics capable of neutralizing the bases (e.g., alkylamines and ammonia) after oxidation to organic acids by IOPs. These reactions decrease the particle-phase mole fractions of the higher-volatility reactants, serving to drive more reactants into the particle phase. The formation of highly hygroscopic alkylaminium salts can further promote the particle growth ultimately to CCN through condensation of water and water-soluble secondary compounds (e.g., glyoxal). These results suggest strongly that higher iodine oxides and organics act synergistically in marine new particle formation, particularly at the early stage of particle growth.

The growth-factors driven by heterogeneous reactions in the single and dual component systems can be expressed in terms of an equivalent vapor concentration enhancement. For example, for both IOP-dimethylamine and IOP-meso-erythritol systems, the growth-factor associated with the smallest seed particles (6 nm) is 1.1, corresponding to a condensed volume increase of 33%. Similarly, the dual component heterogeneous system of IOP-dimethylamine-meso-erythritol leads to a growth-factor of 1.43, corresponding to a condensed volume increase of 192%, equating to 5.8 times that of the single-component systems. Thus, the accelerated growth rate in the dual component heterogeneous reaction system relative to the single component system effectively amplifies the vapor concentration by a factor of 5.8. Likewise, for the largest seed particles (20 nm), the equivalent vapor concentration is 5.6 times higher than the dimethylamine concentration and 3.4 times higher than the meso-erythritol concentration (dimethylamine has a growth-factor of 1.2 and meso-erythritol 1.32). The lower growth-factor for the smaller seed particles is a consequence of the Kelvin effect. The observed growth-factors were replicated using a basic model for condensation growth and heterogeneous reactions that, when applied to the single and dual component systems, demonstrates that for the single component system, the growth is rate-limited by condensation, whereas the dual component system is rate-limited by the heterogeneous reactions. Effectively, growth via single component heterogeneous reactions is similar to growth via condensation; however, the remarkable enhancement in growth occurs in the dual component system. For the dimethylamine-glyoxal system, the equivalent vapor concentration enhancements are 7–8 times higher than that for the single vapor concentrations with the smallest seeds (8 nm) and 3–6 times higher for the 15 nm seeds. If one compares this to a system with two noninteracting vapors condensing simultaneously, the enhancement is halved. In summary, these results reveal that IOP undergoing heterogeneous reactions with dual-component organic vapors leads to accelerated nano-particle

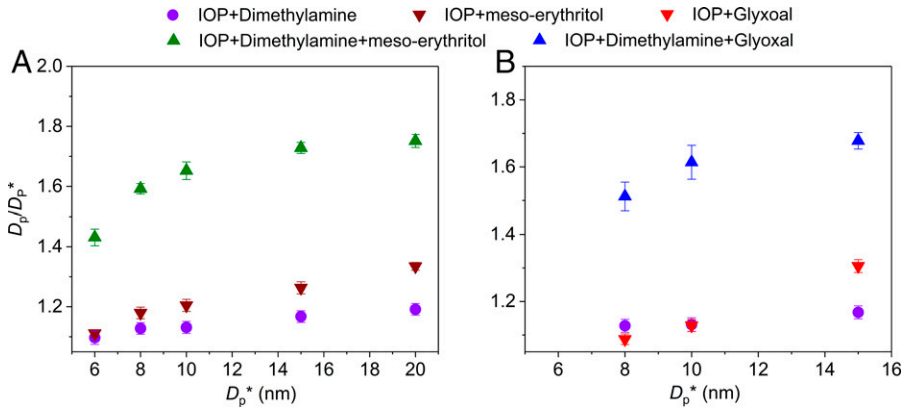

Fig. 2. Particle growth factor (GF, D_P/D_P*) for IOP seed particles exposed to different organic vapors. (*A*) On exposure to dimethylamine, meso-erythritol, and dimethylamine + meso-erythritol, respectively. (*B*) On exposure to dimethylamine, glyoxal, and dimethylamine + glyoxal, respectively. The uncertainty bars represent two SDs of all measurements (2σ).

growth rates from a factor of 3 to a factor of 8. Such an increase in particle growth rate, or particle size for sub-10 nm particles, can increase the particle survival rate against diffusive coagulative loss by more than an order of magnitude (30), ultimately leading to a significant increase in background marine aerosol particle and CCN concentration.

Chemical Evolution of Particle and Recycling of Iodine. The heterogeneous reactions of organics with higher iodine oxides, releasing iodine from the aerosol phase, are a potentially significant contribution to the inorganic iodine pool. We explored the potential for this recycling through laboratory experiments into the aqueous-phase reactions involving higher iodine oxides (specifically, I_2O_5, in hydrolyzed form IO_3^-) and selected organic vapors (e.g., alcohols and aldehydes) using atmospheric pressure chemical ionization–mass spectrometry (APCI-MS) in negative-ion mode. After introducing the higher-IOPs into the ion source, an intensive signal of the IO_3^--ion is visible (Fig. 3*A*). Upon introduction of the organics into the aqueous iodate particles, a rapid increase in the *m*/*z* ratio 254 (I_2^-) is observed, an unambiguous indication of the reduction of iodate by the alcohol (e.g., meso-erythritol). As molecular iodine is formed, the iodate signal decreases simultaneously, indicating the consumption of iodate. Similar results are observed for other alcohols (*SI Appendix*, Fig. S6).

A further set of experiments shows that organics with hydroxyl (−OH) or formyl (−CHO) functional groups can be oxidized by higher iodine oxides to form corresponding ketones, aldehydes or carboxylic acids. The resulting molecular iodine released into the gas phase, as quantified using a diffusion denuder-GC/MS method (31), is a significant proportion of the particulate iodine (see Fig. 3*B*). The amount of I_2 released is controlled by the alcohol/iodine oxide ratio and pH of the aerosol particles. More I_2 is released with increasing alcohol/I_2O_5 ratio and pH value (pH 2–6), as illustrated in *SI Appendix*, Figs. S7 and S8, respectively. This suggests that the cycles of higher iodine oxides occur irrespective of the temporal and spatial variability of condensable organic species as well as the pH value in each aerosol particle.

Although, due to instrument limitations, the reduction of iodate was not detectable in the nascent open ocean nucleation event presented here (Fig. 1), the evolution of organics is strikingly consistent with the laboratory studies. It should be noted that ambient measurements can rarely provide a "smoking gun" due to the multiplicity of overlapping processes and sensitivity of even state-of-the-art instruments employed for ultrafine particle measurements, however, the observations discussed in this study provide strong support and are highly consistent with concept of heterogeneous iodine-organic chemistry facilitating and accelerating new particle production and growth. While ambient measurements did not show the specific size range of 6–20 nm tested in the laboratory studies, it is reasonable to believe that the heterogeneous iodine-organic chemistry is also applicable to ∼30–60 nm range observed in marine air. Ultrafine mode mass spectra (see *SI Appendix*, Fig. S9) show a significant increase in di-carbonyls and oxoacid contribution (*m*/*z* 29 and 44) with the growth of the particles and concurrent reduction in other species such as alkenes, cyclic alcohols, or cycloalkyl carbonyls (C_nH_{2n-1}/$C_nH_{2n-1}CO$: *m*/*z* 41, 55). Observations of these products are consistent with the theoretical reactions of iodate with alcohols/aldehydes to form organic acids and with the laboratory results discussed above. Moreover, the fragmentation pattern of the ultrafine mode is reminiscent of iminium salts that can produce CHN and groups of $C_nH_{2n-1}CO$ or C_nH_{2n-3} while fragmenting in the high-resolution AMS. This observation supports the reactions of organic acids or iodate with amines to form salts, as shown above. The presence of I (*m*/*z* 126.9) and CHN (*m*/*z* 27.01) in the ultrafine mode was confirmed by the high-resolution AMS measurements (*SI Appendix*, Figs. S4 and S9); however, it is not possible yet to quantitatively assess ions in this mode. Iminium salts are very good surfactants, consistent with highly efficient CCN activation of these ultrafine particles (32). Populating the Van Krevelen diagram, shown in Fig. 1*C*, with these data through all the phases of growth, reveals a highly oxidized organic state from the very onset of the observed particle event, which is consistent with the heterogeneous oxidation processes. The slope in Fig. 1*C* is shallower than that for carboxylic acid, but it moves toward that direction with particle growth. The shallower slope could result from a net addition of both carboxylic acid and alcohol functional groups without fragmentation, and/or the addition of carboxylic acid groups with fragmentation (33). Laboratory studies presented here point to the latter process.

Discussion

The heterogeneous processes of iodine with organics provide an explanation for the depletion of iodate observed in the MBL (34) and reduce the discrepancy between measured and predicted particulate iodine chemistry (35). This mechanism may

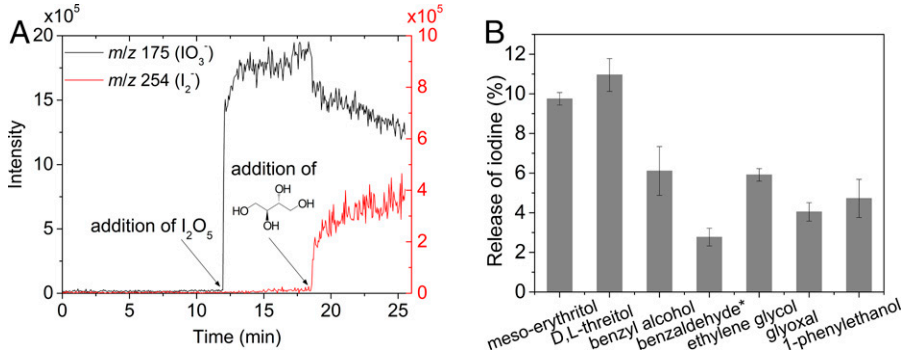

Fig. 3. Particle chemical evolution during the growth from laboratory experiments. (*A*) Reaction of I_2O_5 with meso-erythritol monitored by online APCI-MS analysis. I_2O_5 hydrolyzed in aerosol water leading to the production of IO_3^-, which can be seen from the *m/z* 175 signal. IO_3^- was rapidly reduced to form I_2 upon introduction of meso-erythritol into the reaction system, inferred from a rapid decrease of IO_3^- signal and increase of I_2^- (*m/z* 254) signal. (*B*) Quantification of the released I_2 formed from IO_3^- (product of I_2O_5 hydrolysis) reduction by alcohols or aldehydes in the particle phase. The molar ratio of organic/I_2O_5 is 100:1 except for benzaldehyde (50:1), and the pH of bulk solution is ~3. Errors (2σ) ranged between 3.3% and 20.4% and were determined from triplicate runs of three individual experiments for each reaction.

also provide a pathway to transport reactive iodine species (e.g., I_2 and IO) to more remote areas of the atmosphere because iodine-containing particles have much longer lifetime compared to I_2 and function like a "carrier" from which reactive iodine species can be recycled during atmospheric transport. This process, together with heterogeneous uptake of HOI onto chloride- and bromide-containing sea-salt aerosols to release ICl and IBr (36–38), may provide a significant contribution to the inorganic iodine pool, with further modeling work needed to assess the global atmospheric relevance of iodine-organic heterogeneous chemistry.

Accelerated growth of IOP through heterogeneous reaction pathways and the transport and subsequent recycling of iodine bring critical strands to our conceptual understanding of new particle formation in the marine environment. It has previously been demonstrated that, while there are sufficient iodine oxide vapors in the remote MBL to promote nucleation, condensable organic vapors at concentrations in excess of 10^7 cm^{-3} are required to grow the seed particles into quasi-stable aerosol particles that can ultimately become CCN. The dual-component heterogeneous reaction systems presented here suggest that this critical growth process can occur at effective organic vapor concentrations an order of magnitude lower than that required for condensation processes. Thus, the heterogenous system leads to "fast-tracking" of new particle formation in the MBL, ultimately leading to an increase in the background marine aerosol.

Fig. 4 summarizes the proposed conceptual strands in context of new particle formation in the MBL. Iodine compounds (I_2, VOI) are released in biologically active regions (induced by biotic or abiotic processes) from the sea surface into the MBL, photolyzed and oxidized to form iodine oxides or iodine oxoacids (HIO_3 and HIO_2). The nucleation rates of HIO_3 are rapid, even exceeding sulfuric acid-ammonia rates under similar conditions (39), while if the concentrations of the iodine oxides are sufficiently high, their self-reactions lead to higher oxidized iodine oxides for which new particle formation induced by IOPs can occur (4, 40). At lower iodine oxide concentrations, iodine compounds are still likely to contribute to the early cluster growth by chemical activation of the prenucleation cluster. Within the recently formed ultrafine particles, the reactions between the higher iodine oxides and the condensing alcohols or carbonyls (IOOs) lead to formation of low volatility oxidized organics where the produced organic acids can further react with basic molecules (e.g., amines) to form highly hygroscopic salts, accelerating early particle growth into the Aitken mode. By further condensational growth and heterogeneous iodine-organic chemistry, the particles ultimately reach CCN sizes. Either at this or at an earlier stage, the higher iodine oxides are recycled, restarting the reaction sequence. In this way, iodine acts as a "catalyst" for nucleation and subsequent new particle formation in marine air.

Materials and Methods

Marine Air Observation. The ambient measurements are continuously undertaken at the Mace Head Global Atmosphere Watch Research Station, located on the west coast of Ireland. Over a period of 10 y (2008–2018), we observed over 80 open ocean new particle formation events with steady growth lasting longer than 6 h under clean marine conditions. These events occurred in marine air masses with 57% of occurrence in *mP*, 36% of *mA*, and 17% of *mT* air masses. The event, discussed in this study, occurred in June 2012 and lasted for over 36 h. It manifested in the *mP* air mass without major land contact for at least 48 h (see *SI Appendix*, Fig. S2) as derived from 3-d back trajectories calculated

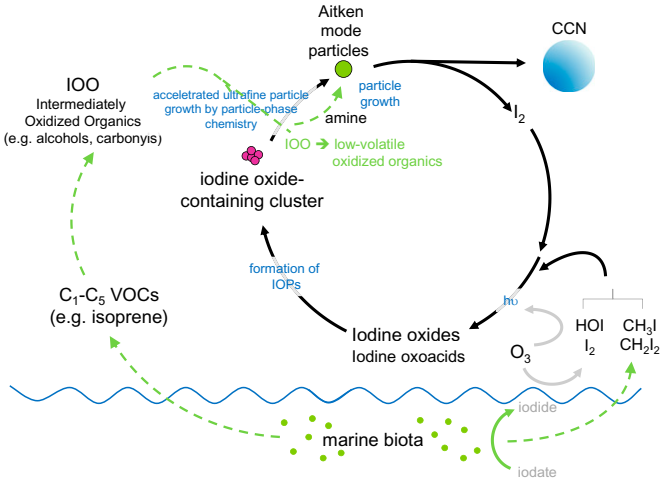

Fig. 4. Insights into iodine-organic multiphase reactions fast-tracking marine new particle formation. Iodine released from the ocean surface is photolyzed and oxidized to form iodine oxides or iodine oxoacids (HIO_3 and HIO_2), which can nucleate to form IOPs or contribute to the early cluster growth by chemical activation of the prenucleation cluster. Within the recently formed ultrafine particles heterogeneous reactions between the higher iodine oxides and condensing alcohols or carbonyls from oxidation of marine VOCs lead to the formation of low volatility oxidized organics where the produced organic acids can further react with basic molecules (e.g., amines) to form highly hygroscopic salts, accelerating the early particle growth into Aitken mode and ultimately CCN. During this process, the higher iodine oxides are recycled, restarting the reaction sequence.

using the Hybrid Single-Particle Lagrangian Integrated Trajectory transport and dispersion model. The event is characteristic of "open ocean new particle production events" as previously classified by O'Dowd et al. (11).

Aerosol size distributions were measured using a SMPS system. The system comprised a differential mobility analyzer (DMA, TSI model 3071), a condensation particle counter (TSI model 3010), and an aerosol neutralizer (TSI 3077). The SMPS system follows the European Supersites for Atmospheric Aerosol Research protocol for particle physical properties measurement and is regularly calibrated according to these guidelines.

Aerosol chemical composition was measured using an Aerodyne HR-ToF-AMS (42). The HR-ToF-AMS was routinely calibrated according to the methods described in Allan et al. (43). The measurements were performed at a time resolution of 5 min and a vaporizer temperature of ∼650 °C. Although standard 1-min resolution detection limits (DL) are 22, 5.2, 2.9, 38, and 12 ng m^{-3} for organic matter (OM), sulfate, nitrate, ammonium, and chloride, respectively (42), averaging over a 12-h period results in a 10-fold improvement in DL: 6, 1.5, 0.9, 7, and 1.2 ng m^{-3} for OM, sulfate, nitrate, ammonium, and chloride, respectively (32).

All aerosol instruments were connected to the main community sampling system while retaining isokinetic flows. The main sampling system is constructed from a 100 mm diameter stainless steel pipe with the main inlet at 10 m above ground level. The performance of this inlet is described in Kleefeld et al. (44).

Nanoparticle Growth. *SI Appendix*, Fig. S10 shows the schematic of experimental set-up for nanoparticle growth measurement. Nano-sized IOPs (2–50 nm) were produced by homogeneous nucleation of iodine oxides formed from photochemistry of I_2 with O_3 in a laminar-flow aerosol chamber or by nebulization of I_2O_5 aqueous solution which gave higher IOP concentrations and thereby sufficient mass of reaction products for subsequent TD-ID-CIMS analysis. The size distribution and number concentration of IOPs were adjustable from the concentrations of I_2, O_3, and H_2O (or relative humidity) and were measured using a combination of DMA and an ultrafine condensation particle counter. The aerosol flow from the nucleation chamber was first mixed with a humidified nitrogen flow to regulate the relative humidity, with a typical uncertainty of 2%. IOPs were size-selected using the first nano-tandem DMA (D_p*) and, subsequently, introduced into the growth chamber (1.5 m length × 2.54 cm inside diameter), where they were exposed to organic vapors. The second nano-tandem DMA was used to sample the aerosol flow at the end of the growth chamber (D_p) and the ratio of the particle sizes measured by these two nano-tandem DMAs yielded the particle growth factor (D_p/D^*_p). Organic vapors were introduced into the aerosol growth chamber at a flow rate of 300 mL min^{-1} and at a relative humidity identical to that of the sample flow. A flow of 300 mL min^{-1} was removed at the end of the growth chamber using a critical orifice. The concentrations of meso-erythritol and dimethylamine in the growth chamber were estimated to be 2.9 × 10^{14} and 8.0 × 10^{12} molecules cm^{-3}, respectively, and the concentration of glyoxal was determined to be 1.2 × 10^{14} molecules cm^{-3} by a 552 UV-visible spectrophotometer (Pekin-Elmer). The concentrations of organic vapors used in our experiments were higher than those in ambient air but were necessary to achieve measurable growth factors because of a shorter reaction time in our experiments.

Characterization of Organics Formed from Heterogeneous Reaction. TD-ID-CIMS was used to analyze the products formed from heterogeneous reactions after exposure of IOPs to organic vapors. The aerosols from the growth chamber were collected using an electrostatic precipitator, and subsequently thermally desorbed at 300 °C and analyzed using TD-ID-CIMS. The reagent ions H_3O^+ and CO_3^-/CO_4^- were used for all analyses. The collected particles were size-resolved (2–50 nm), with a typical size of 10 nm. For a typical experiment, a time of ∼2 h was used to collect 1–2 ng particles by assuming a 10% overall charging efficiency over the 2–50 nm range and a particle density of 1.5 g cm^{-3} at the aerosol flow rate of 3.0 L min^{-1}.

Model Simulation. The growth of particles was simulated with an aerosol model that resolves the mass transfer for dimethylamine, meso-erythritol, and glyoxal from the gas phase to IOP particles by condensation, evaporation, and chemical reactions concurrently, using the variable coefficient ODE Solver (45). The model structure follows that described by Kokkola et al. (46). The chemical reactions considered in the model include:

$$\mathrm{IOP} + \mathrm{H_2O} \rightarrow \mathrm{HIO_3}, \quad (1)$$

$$\mathrm{HIO_3} + \text{dimethylamine} \rightarrow \text{salt (low volatility/non-volatile)}, \quad (2)$$

$$\text{glyoxal (or meso-erythritol)} + \mathrm{HIO_3} \rightarrow \text{organic acid (water soluble, low volatility)}, \quad (3)$$

and

$$\text{organic acid} + \text{dimethylamine} \rightarrow \text{salt (non-volatile, stable salt)}. \quad (4)$$

Identification and Quantification of Iodine. Aerosol particles were generated continuously by nebulizing a mixture of aqueous solution at a flow rate of 1,600 mL min^{-1}. To minimize reactions in bulk solution the I_2O_5 aqueous solution was mixed (ratio 1.2:1, vol/vol) with another organic compound containing aqueous solution, which was delivered by a peristaltic pump, in a T-connector that was mounted very close (∼0.1 cm) to the atomizer cell. The resulting aqueous particles passed through a diffusion dryer and then sampled into the online APCI-MS (Finnigan LCQ, IT-MS, Finnigan MAT) operated in negative mode with a modified APCI ion source for identification analysis (47) or flowed into a 10 L flow tube for further aging. The flow tube outflow was sampled by a coupled diffusion denuder system for 10–30 min at a flow rate of 500 mL min^{-1} for collecting the released I_2, followed by analysis using a gas chromatography–mass spectrometry method (31). The total concentration of iodine in the generated particles was measured with inductively coupled plasma mass spectrometry after particle collection using a combined wet effluent diffusion denuder-steam jet aerosol collector (EDD-SJAC). Any I_2 that may have been released from particles at the sampling line between sampling port and SJAC was collected by the EDD using 10 μg mL^{-1} of 1,3,5-trimethoxybenzene aqueous solution. The entire experimental system was protected from any adventitious light by Al foil.

Data Availability. All study data are included in the article and/or *SI Appendix*. Data related to this article are also available at the East Asian Paleoenvironmental Science Database, National Earth System Science Data Center, National Science & Technology Infrastructure of China (http://paleodata.ieecas.cn/index.aspx) (48).

ACKNOWLEDGMENTS. The authors gratefully acknowledge the NOAA Air Resources Laboratory (ARL) for the provision of the HYSPLIT transport and dispersion model used in this publication. This work was supported by the National Natural Science Foundation of China (41925015), the Key Research Program of Frontier Sciences from the Chinese Academy of Sciences (ZDBS-LY-DQC001), the Strategic Priority Research Program of the Chinese Academy of Sciences (XDB40000000), SKLLQG (SKLLQGTD1801), the European Union's Seventh Framework Programme (FP7/2007-2013) project BACCHUS under grant agreement 603445, the Irish Environmental Protection Agency, the HEA PRTLI4 project, and MaREI, the SFI (Science Foundation Ireland) Research Centre for Energy, Climate and Marine.

Author affiliations: [a]State Key Laboratory of Loess and Quaternary Geology, Center for Excellence in Quaternary Science and Global Change, Institute of Earth Environment, Chinese Academy of Sciences, Xi'an 710061, China; [b]Open Studio for Oceanic-Continental Climate and Environment Changes, Pilot National Laboratory for Marine Science and Technology (Qingdao), Qingdao 266000, China; [c]Institute of Global Environmental Change, Xi'an Jiaotong University, Xi'an 710049, China; [d]University of Chinese Academy of Sciences, Beijing 100039, China; [e]Department of Chemistry, Johannes Gutenberg University of Mainz, 55128 Mainz, Germany; [f]School of Physics, Ryan Institute's Centre for Climate and Air Pollution Studies, National University of Ireland Galway, Galway H91 CF50, Ireland; [g]Finnish Meteorological Institute, 00560 Helsinki, Finland; [h]Department of Applied Physics, University of Eastern Finland, 70210 Kuopio, Finland; [i]Department of Atmospheric Sciences, Texas A&M University, College Station, TX 77843; [j]Department of Chemistry, Texas A&M University, College Station, TX 77843; [k]Division of Chemistry and Chemical Engineering, California Institute of Technology, Pasadena, CA 91125; and [l]Division of Engineering and Applied Science, California Institute of Technology, Pasadena, CA 91125

1. S. Schobesberger *et al.*, Molecular understanding of atmospheric particle formation from sulfuric acid and large oxidized organic molecules. *Proc. Natl. Acad. Sci. U.S.A.* **110**, 17223–17228 (2013).
2. J. Almeida *et al.*, Molecular understanding of sulphuric acid-amine particle nucleation in the atmosphere. *Nature* **502**, 359–363 (2013).
3. M. Sipilä *et al.*, Molecular-scale evidence of aerosol particle formation via sequential addition of HIO_3. *Nature* **537**, 532–534 (2016).
4. J. C. Gómez Martín *et al.*, A gas-to-particle conversion mechanism helps to explain atmospheric particle formation through clustering of iodine oxides. *Nat. Commun.* **11**, 4521 (2020).

5. R.-J. Huang *et al.*, Observations of high concentrations of I_2 and IO in coastal air supporting iodine-oxide driven coastal new particle formation. *Geophys. Res. Lett.* **37**, L03803 (2010).
6. A. Saiz-Lopez *et al.*, Atmospheric chemistry of iodine. *Chem. Rev.* **112**, 1773–1804 (2012).
7. J. D. Allan *et al.*, Iodine observed in new particle formation events in the Arctic atmosphere during ACCACIA. *Atmos. Chem. Phys.* **15**, 5599–5609 (2015).
8. L. J. Beck *et al.*, Differing mechanisms of new particle formation at two Arctic sites. *Geophys. Res. Lett.* **48**, e2020GL091334 (2021).
9. A. Baccarini *et al.*, Frequent new particle formation over the high Arctic pack ice by enhanced iodine emissions. *Nat. Commun.* **11**, 4924 (2020).
10. C. Prados-Roman *et al.*, Iodine oxide in the global marine boundary layer. *Atmos. Chem. Phys.* **15**, 583–593 (2015).
11. C. O'Dowd, C. Monahan, M. Dall'Osto, On the occurrence of open ocean particle production and growth events. *Geophys. Res. Lett.* **37**, L19805 (2010).
12. K. Sellegri *et al.*, Evidence of atmospheric nanoparticle formation from emissions of marine microorganisms. *Geophys. Res. Lett.* **43**, 6596–6603 (2016).
13. C. A. Cuevas *et al.*, Rapid increase in atmospheric iodine levels in the North Atlantic since the mid-20th century. *Nat. Commun.* **9**, 1452 (2018).
14. K. A. Read *et al.*, Extensive halogen-mediated ozone destruction over the tropical Atlantic Ocean. *Nature* **453**, 1232–1235 (2008).
15. A. S. Mahajan *et al.*, Measurement and modelling of tropospheric reactive halogen species over the tropical Atlantic Ocean. *Atmos. Chem. Phys.* **10**, 4611–4624 (2010).
16. C. Monahan, H. Vuollekoski, M. Kulmala, C. O'Dowd, Simulating marine new particle formation and growth using the M7 modal aerosol dynamics modal. *Adv. Meteorol.* **2010**, 689763 (2010).
17. C. Kuang, P. H. McMurry, A. V. McCormick, Determination of cloud condensation nuclei production from measured new particle formation events. *Geophys. Res. Lett.* **36**, L09822 (2009).
18. D. M. Westervelt *et al.*, Formation and growth of nucleated particles into cloud condensation nuclei: Model–measurement comparison. *Atmos. Chem. Phys.* **13**, 7645–7663 (2013).
19. M. Claeys *et al.*, Formation of secondary organic aerosols through photooxidation of isoprene. *Science* **303**, 1173–1176 (2004).
20. M. M. Galloway *et al.*, Yields of oxidized volatile organic compounds during the OH radical initiated oxidation of isoprene, methyl vinyl ketone, and methacrolein under high-NOx conditions. *Atmos. Chem. Phys.* **11**, 10779–10790 (2011).
21. S. L. Shaw, B. Gantt, N. Meskhidze, Production and emissions of marine isoprene and monoterpenes: A review. *Adv. Meteorol.* **2010**, 408696 (2010).
22. J. E. Krechmer *et al.*, Formation of low volatility organic compounds and secondary organic aerosol from isoprene hydroxyhydroperoxide low-NO oxidation. *Environ. Sci. Technol.* **49**, 10330–10339 (2015).
23. J. R. Pierce *et al.*, Quantification of the volatility of secondary organic compounds in ultrafine particles during nucleation events. *Atmos. Chem. Phys.* **11**, 9019–9036 (2011).
24. S. D. D'Andrea *et al.*, Understanding global secondary organic aerosol amount and size-resolved condensational behavior. *Atmos. Chem. Phys.* **13**, 11519–11534 (2013).
25. M. Ehn *et al.*, A large source of low-volatility secondary organic aerosol. *Nature* **506**, 476–479 (2014).
26. J. Tröstl *et al.*, The role of low-volatility organic compounds in initial particle growth in the atmosphere. *Nature* **533**, 527–531 (2016).
27. L. Wang *et al.*, Atmospheric nanoparticles formed from heterogeneous reactions of organics. *Nat. Geosci.* **3**, 238–242 (2010).
28. M. Rinaldi *et al.*, Evidence of a natural marine source of oxalic acid and a possible link to glyoxal. *J. Geophys. Res.* **116**, D16204 (2011).
29. S. Myriokefalitakis *et al.*, In-cloud oxalate formation in the global troposphere: A 3-D modeling study. *Atmos. Chem. Phys.* **11**, 5761–5782 (2011).
30. C. D. O'Dowd *et al.*, Marine aerosol formation from biogenic iodine emissions. *Nature* **417**, 632–636 (2002).
31. R.-J. Huang, T. Hoffmann, Development of a coupled diffusion denuder system combined with gas chromatography/mass spectrometry for the separation and quantification of molecular iodine and the activated iodine compounds iodine monochloride and hypoiodous acid in the marine atmosphere. *Anal. Chem.* **81**, 1777–1783 (2009).
32. J. Ovadnevaite *et al.*, Surface tension prevails over solute effect in organic-influenced cloud droplet activation. *Nature* **546**, 637–641 (2017).
33. N. L. Ng *et al.*, Changes in organic aerosol composition with aging inferred from aerosol mass spectra. *Atmos. Chem. Phys.* **11**, 6465–6474 (2011).
34. A. R. Baker, Inorganic iodine speciation in tropical Atlantic aerosol. *Geophys. Res. Lett.* **31**, L23S02 (2004).
35. S. Pechtl, G. Schmitz, R. von Glasow, Modelling iodide–iodate speciation in atmospheric aerosol: Contributions of inorganic and organic iodine chemistry. *Atmos. Chem. Phys.* **7**, 1381–1393 (2007).
36. R. Vogt, P. J. Crutzen, R. Sander, A mechanism for halogen release from sea-salt aerosol in the remote marine boundary layer. *Nature* **383**, 327–330 (1996).
37. C. F. Braban *et al.*, Heterogeneous reactions of HOI, ICl and IBr on sea salt and sea salt proxies. *Phys. Chem. Chem. Phys.* **9**, 3136–3148 (2007).
38. Y. J. Tham *et al.*, Direct field evidence of autocatalytic iodine release from atmospheric aerosol. *Proc. Natl. Acad. Sci. U.S.A.* **118**, e2009951118 (2021).
39. X. C. He *et al.*, Role of iodine oxoacids in atmospheric aerosol nucleation. *Science* **371**, 589–595 (2021).
40. J. C. Gómez Martín *et al.*, On the mechanism of iodine oxide particle formation. *Phys. Chem. Chem. Phys.* **15**, 15612–15622 (2013).
41. C. L. Heald *et al.*, A simplified description of the evolution of organic aerosol composition in the atmosphere. *Geophys. Res. Lett.* **37**, L08803 (2010).
42. P. F. DeCarlo *et al.*, Field-deployable, high-resolution, time-of-flight aerosol mass spectrometer. *Anal. Chem.* **78**, 8281–8289 (2006).
43. J. D. Allan *et al.*, Quantitative sampling using an Aerodyne aerosol mass spectrometer: 1. Techniques of data interpretation and error analysis. *J. Geophys. Res.* **108**, 4090 (2003).
44. C. Kleefeld *et al.*, Relative contribution of submicron and supermicron particles to aerosol light scattering in the marine boundary layer. *J. Geophys. Res.* **107**, 8103 (2002).
45. P. N. Brown, G. D. Byrne, A. C. Hindmarsh, VODE: A variable coefficient ODE solver. *SIAM J. Sci. Statist. Comput.* **10**, 1038–1051 (1989).
46. H. Kokkola, S. Romakkaniemi, M. Kulmala, A. Laaksonen, A cloud microphysics model including trace gas condensation and sulfate chemistry. *Boreal Environ. Res.* **8**, 413–424 (2003).
47. U. Kückelmann, B. Warscheid, T. Hoffmann, On-line characterization of organic aerosols formed from biogenic precursors using atmospheric pressure chemical ionization mass spectrometry. *Anal. Chem.* **72**, 1905–1912 (2000).
48. R.-J. Huang *et al.*, Data for "Heterogeneous iodine-organic chemistry fast-tracks marine new particle formation." East Asian Paleoenvironmental Science Database. http://paleodata.ieecas.cn/FrmDataInfo_EN.aspx?id=fdebe391-9800-40d0-b022-4ac5f20ce101. Accessed 29 July 2022.